Nonlinear Dyn (2012) 67:1539–1557
DOI 10.1007/s11071-011-0087-2

ORIGINAL PAPER

Integrated mechanical and control design of underactuated multibody systems

Robert Seifried

Received: 3 September 2010 / Accepted: 12 May 2011 / Published online: 10 June 2011

Abstract Multibody systems are called underactuated if they have less control inputs than degrees of freedom, e.g. due to passive joints or body flexibility. For trajectory tracking of underactuated multibody systems often advanced modern nonlinear control techniques are necessary. The analysis of underactuated multibody systems might show that they possess internal dynamics. Feedback linearization is only possible if the internal dynamics remain bounded, i.e. the system is minimum phase. Also feed-forward control design for minimum phase systems is much easier to realize than for non-minimum phase systems. However, often the initial design of an underactuated multibody system is non-minimum phase. Therefore, in this paper a procedure for integrated mechanical and control design is proposed such that minimum phase underactuated multibody systems are obtained. Thereby an optimization-based design process is used, whereby the geometric dimensions and mass distribution of the multibody systems are altered.

Keywords Multibody systems · Underactuation · Internal dynamics · Minimum phase · Feedback linearization · System design · Particle swarm optimization

R. Seifried (✉)
Institute of Engineering and Computational Mechanics, University of Stuttgart, Pfaffenwaldring 9, 70569 Stuttgart, Germany
e-mail: robert.seifried@itm.uni-stuttgart.de

1 Introduction

Underactuated multibody systems have less control inputs than degrees of freedom. Typical underactuated multibody systems are manipulators with body flexibility or joint elasticity, systems with passive joints and crane structures. Underactuated systems become increasingly important in modern system designs. For example body flexibility often arises in modern energy efficient fast moving light weight manipulators. Also passive joints might be used to reduce the number of actuators and therefore reduce the total mass of a system to decrease the energy consumption. Also passive joints might arise due to actuator failure or might be used intentionally to introduce compliance. In the case of underactuation the controller design is often much more involved than in the fully actuated case. For example for end-effector trajectory tracking the method of computed torque known from fully actuated systems, see e.g. [2, 23], cannot be used due to the underactuation. Thus, for trajectory tracking of underactuated multibody systems generally more advanced modern nonlinear control techniques are necessary.

Feedback linearization is a nonlinear control technique based on differential-geometric concepts which is well suited for output trajectory tracking [4, 7, 13, 22]. These concepts can also be used for feedforward control design [13], which can be used in a two-degree of freedom control structure. Using these nonlinear control concepts the analysis of the mechanical design of underactuated multibody systems might

show that they possess internal dynamics. Internal dynamics arise for example often in the case of flexible manipulators [5, 12, 18] or in multibody systems with passive joints [11, 20]. In contrast manipulators with joint elasticity [5] and cranes [3] are often differentially flat, possessing no internal dynamics. This paper focus on the first case, namely multibody systems with internal dynamics.

Using feedback linearization this internal dynamics is rendered unobservable and its behavior must be analyzed carefully to guarantee that it remains bounded. Therefore, often the concept of zero dynamics is used. This is the internal dynamics under the constraint of constant zero output. Systems with asymptotically stable zero dynamics are called minimum phase, otherwise non-minimum phase. Only for minimum phase systems feedback linearization is possible. Also in this case the design of feed-forward control is rather straight forward [19]. Conversely, for non-minimum phase systems feedback linearization is not possible. Also in this case feed-forward control design is much more complex and requires the numerical solution of a two-sided boundary value problem, see [6, 18, 20, 24].

Due to these difficulties the aim should be to design an underactuated multibody system in such a way that it is minimum phase. Therefore, in this paper an integrated mechanical and control design process is proposed. Thus, already in the early state of the design process mechanical design and control design are considered concurrently. This integrated design approach is based on an optimization procedure for the mechanical design. Thus, underactuated multibody systems with bounded internal dynamics are designed. In [1] a similar design methodology is used to design differentially flat underactuated planar manipulators by using a special mass distribution. In this case, no internal dynamics remains and full-state linearization is possible; however, the approach might require the use of larger counterweights.

In the proposed optimization procedure, the design parameters are identified as the geometric dimensions and mass distribution of the multibody systems. Different design parameterizations such as the use of small counterweights are proposed. It is shown that minimum phase property can be achieved with only a modest or no increase of the total mass of the underactuated multibody systems. For computational efficiency the proposed optimization criteria has two steps and firstly requires that all eigenvalues of the linearized zero dynamics are in the left half-plane, and secondly that initial errors in the nonlinear zero dynamics decay rapidly. The analysis of this optimization problem shows that it is discontinuous and local minima might exist. Therefore, a particle swarm optimization procedure is used. This optimization-based design approach is demonstrated by simulations for manipulators with two and four passive joints, respectively. The comparison with alternative control strategies of the initial non-minimum phase design shows the efficiency of the proposed integrated design approach; and also its robustness is demonstrated by simulation.

The paper is organized in the following way. In Sect. 2 the trajectory tracking control design for underactuated multibody systems is described. Thereby also a linearly combined system output is introduced in order to simplify the analysis of the internal dynamics. In Sect. 3 the optimization procedure for designing minimum phase systems is discussed. In Sect. 4 application examples are presented, before the findings of the paper are summarized in Sect. 5.

2 Trajectory tracking control

The equation of motion in minimal coordinates of a multibody system with f degrees of freedom and generalized coordinates $\boldsymbol{q} \in \mathbb{R}^f$ is given by

$$\boldsymbol{M}(\boldsymbol{q})\ddot{\boldsymbol{q}} + \boldsymbol{k}(\boldsymbol{q}, \dot{\boldsymbol{q}}) = \boldsymbol{g}(\boldsymbol{q}, \dot{\boldsymbol{q}}) + \boldsymbol{B}(\boldsymbol{q})\boldsymbol{u}. \tag{1}$$

Thereby $\boldsymbol{M} \in \mathbb{R}^{f\times f}$ is the mass matrix, $\boldsymbol{k} \in \mathbb{R}^f$ the vector of generalized gyroscopic and centrifugal forces, and $\boldsymbol{g} \in \mathbb{R}^f$ the vector of applied forces. The input matrix $\boldsymbol{B} \in \mathbb{R}^{f\times m}$ distributes the m control inputs $\boldsymbol{u} \in \mathbb{R}^m$ onto the f directions of the generalized coordinates. The multibody system has the system output

$$\boldsymbol{y} = \boldsymbol{h}(\boldsymbol{q}), \tag{2}$$

where it is generally assumed that the number of system outputs and control inputs agree, i.e. $\boldsymbol{y} \in \mathbb{R}^m$. For a multibody system the system output could be an end-effector position $\boldsymbol{r}^{\mathrm{ef}}(\boldsymbol{q})$ which should track a predefined trajectory.

In the case of a fully actuated multibody system there are as many control inputs as generalized coordinates, i.e. $m = f$. Then, the equation of motion can be inverted by algebraic manipulations; and classical

computed torque can be used for trajectory tracking control, see e.g. [2, 23]. In contrast, if the multibody system has less control inputs than generalized coordinates, i.e. $m < f$, the system is underactuated. In this case the input matrix $\boldsymbol{B}$ cannot be inverted and the classical approach of computed torque cannot be used. Thus, more advanced nonlinear control techniques are necessary. For the analysis and control design of underactuated multibody systems it is often useful to partition the equation of motion (1) into two parts,

$$\begin{bmatrix} \boldsymbol{M}_{aa} & \boldsymbol{M}_{au} \\ \boldsymbol{M}_{au}^T & \boldsymbol{M}_{uu} \end{bmatrix} \begin{bmatrix} \ddot{\boldsymbol{q}}_a \\ \ddot{\boldsymbol{q}}_u \end{bmatrix} + \begin{bmatrix} \boldsymbol{k}_a \\ \boldsymbol{k}_u \end{bmatrix} = \begin{bmatrix} \boldsymbol{g}_a \\ \boldsymbol{g}_u \end{bmatrix} + \begin{bmatrix} \boldsymbol{B}_a \\ \boldsymbol{B}_u \end{bmatrix} \boldsymbol{u}. \quad (3)$$

Thereby, the submatrix $\boldsymbol{B}_a \in \mathbb{R}^{m \times m}$ has rank m. The first m rows of the partitioned equation of motion (3) are referred to as actuated part associated with the m actuated coordinates $\boldsymbol{q}_a$. The remaining $f - m$ rows are referred to as the unactuated part associated with the $f - m$ unactuated coordinates $\boldsymbol{q}_u$. In the following it is assumed that $\boldsymbol{B}_a = \boldsymbol{I}$ is the identity matrix and $\boldsymbol{B}_u = \boldsymbol{0}$. These special choices represent important cases of underactuated multibody systems in tree structure. Examples include rigid multibody systems with passive joints and planar flexible manipulators, where the shape functions of the flexible bodies are chosen according to clamped boundary conditions, see e.g. [5]. It should be noted that the calculations presented in this paper can also be applied to other cases of $\boldsymbol{B}_a, \boldsymbol{B}_u$.

2.1 Input–output normal-form

The nonlinear input–output normal-form is the basis for feedback linearization as well as for feed-forward control design by exact model inversion. These approaches are based on concepts from differential geometry and its theoretical background is described in [7, 13, 22]. This input–output normal-form is obtained by applying a nonlinear coordinate transformation to the equation of motion. This diffeomorphic coordinate transformation is given by $\boldsymbol{z} = \boldsymbol{\Phi}(\boldsymbol{x})$, where $\boldsymbol{x} = [\boldsymbol{q}^T, \dot{\boldsymbol{q}}^T]^T \in \mathbb{R}^{2f}$ are the original coordinates and $\boldsymbol{z} \in \mathbb{R}^{2f}$ are the coordinates of the input–output normal-form. In general the determination of the new coordinates $\boldsymbol{z}$ requires a state-space representation of the nonlinear system (1) and the symbolic computation of Lie-derivatives of the system output (2), see [7, 13, 22]. However, even for multibody systems with very few degrees of freedom, these necessary symbolic calculations become very complicated. Therefore, in the following they are directly performed on the second-order equation of motion. The first two derivatives of the system output are

$$\dot{\boldsymbol{y}} = \frac{\partial \boldsymbol{h}(\boldsymbol{q})}{\partial \boldsymbol{q}} \dot{\boldsymbol{q}} = \boldsymbol{H}(\boldsymbol{q}) \dot{\boldsymbol{q}}, \quad (4)$$

$$\ddot{\boldsymbol{y}} = \boldsymbol{H}(\boldsymbol{q}) \ddot{\boldsymbol{q}} + \bar{\boldsymbol{h}}(\boldsymbol{q}, \dot{\boldsymbol{q}}), \quad (5)$$

where $\boldsymbol{H}$ is the Jacobian-matrix of the system output and $\bar{\boldsymbol{h}} = \dot{\boldsymbol{H}} \dot{\boldsymbol{q}}$ is its local acceleration. In the expression for $\ddot{\boldsymbol{y}}$ in (5) the second derivative of the generalized coordinates $\ddot{\boldsymbol{q}}$ can be replaced by the equation of motion (1),

$$\begin{aligned} \ddot{\boldsymbol{y}} &= \boldsymbol{H} \ddot{\boldsymbol{q}} + \bar{\boldsymbol{h}} = \boldsymbol{H} \boldsymbol{M}^{-1} [\boldsymbol{g} - \boldsymbol{k} + \boldsymbol{B} \boldsymbol{u}] + \bar{\boldsymbol{h}} \\ &= \boldsymbol{H} \boldsymbol{M}^{-1} \boldsymbol{B} \boldsymbol{u} + \boldsymbol{H} \boldsymbol{M}^{-1} [\boldsymbol{g} - \boldsymbol{k}] + \bar{\boldsymbol{h}}. \end{aligned} \quad (6)$$

If the matrix $\boldsymbol{P} = \boldsymbol{H} \boldsymbol{M}^{-1} \boldsymbol{B}$ is nonsingular the input $\boldsymbol{u}$ can be computed from (6). In this case $\boldsymbol{P}$ is called the decoupling matrix. Then, no further derivatives are necessary and the first part of the coordinate transformation is found. In this case the system is said to have vector relative degree $r = \{r_1, \ldots, r_m\} = \{2, \ldots, 2\}$, since each output is differentiated twice until the input $\boldsymbol{u}$ can be computed. This is typical for many multibody systems with passive joints or flexible bodies. Otherwise, further derivatives might have to be calculated. Examples for this second case are flat mechanical systems such as manipulators with joint elasticities or cranes, see e.g. [3]. For systems with relative degree $r = \{2, \ldots, 2\}$ the nonlinear coordinate transformation is given by

$$\boldsymbol{z} = \boldsymbol{\Phi}(\boldsymbol{x}) = \begin{bmatrix} z_1 \\ z_2 \\ z_3 \end{bmatrix} \quad \begin{aligned} z_1 &= \boldsymbol{y} = \boldsymbol{h}(\boldsymbol{q}) \\ \text{with } z_2 &= \dot{\boldsymbol{y}} = \boldsymbol{H}(\boldsymbol{q}) \dot{\boldsymbol{q}} \\ z_3 &= \boldsymbol{\Phi}_3(\boldsymbol{q}, \dot{\boldsymbol{q}}). \end{aligned} \quad (7)$$

Thereby the coordinates $z_3 \in \mathbb{R}^{2(f-m)}$ must be determined in such a way that $\boldsymbol{z} = \boldsymbol{\Phi}(\boldsymbol{x})$ forms at least a local diffeomorphic coordinate transformation. This requires that the Jacobian-matrix $\boldsymbol{J} = \frac{\partial \boldsymbol{\Phi}(\boldsymbol{x})}{\partial \boldsymbol{x}}$ is nonsingular [7, 13]. If the function $\boldsymbol{h}(\boldsymbol{q})$ contains all actuated coordinates $\boldsymbol{q}_a$ such that $\boldsymbol{H}_a = \frac{\partial \boldsymbol{H}(\boldsymbol{q})}{\partial \boldsymbol{q}_a}$ is regular, then the unactuated coordinates are often a good choice for the coordinates $z_3 = [\boldsymbol{q}_u^T, \dot{\boldsymbol{q}}_u^T]^T$. Applying the coordinate transformation (7) to the equation of motion (1) yields the nonlinear input–output normal-form

$$\boldsymbol{y} = \boldsymbol{z}_1 \tag{8}$$

$$\dot{\boldsymbol{z}}_1 = \boldsymbol{z}_2 \tag{9}$$

$$\begin{aligned}\dot{\boldsymbol{z}}_2 &= \boldsymbol{P}\boldsymbol{u} + \boldsymbol{H}\boldsymbol{M}^{-1}[\boldsymbol{g} - \boldsymbol{k}] + \bar{\boldsymbol{h}} \\ &= \boldsymbol{\beta}(\boldsymbol{z})\boldsymbol{u} + \boldsymbol{\alpha}(\boldsymbol{z})\end{aligned} \tag{10}$$

$$\dot{\boldsymbol{z}}_3 = \boldsymbol{\rho}(\boldsymbol{z}) + \boldsymbol{\sigma}(\boldsymbol{z})\boldsymbol{u}. \tag{11}$$

It should be noted that $\boldsymbol{P}$ and $\boldsymbol{\beta}$ are the same decoupling matrix, however, given in original and new coordinates, respectively. The input–output normal-form consists of two nonlinear subsystems: The first subsystem describes the relationship between the input $\boldsymbol{u}$ and output $\boldsymbol{y}$. It consist of the output equation (8) and the differential equations (9)–(10), which in total have dimension 2 m. The second subsystem (11) of the normal-form describes the so-called internal dynamics and has dimension $2(f-m)$. From this input–output normal-form the analysis of the internal dynamics, feedback linearization and feed-forward control design can be performed. It should be noted that for fully actuated multibody systems no internal dynamics exist and the equation of motion (1) is already in input–output normal-form, if the system output are the generalized coordinates, i.e. $\boldsymbol{y} = \boldsymbol{q}$.

2.2 Feedback linearization

Feedback linearization is very well suited for output trajectory tracking and is based on the presentation of the nonlinear system in the input–output normal-form. Then, nonlinearities in the transformed system (8)–(11) are canceled using state-feedback, resulting in an exactly linearized system or subsystem, see [4, 7, 13, 22]. This approach is fundamentally different from Jacobian linearization, in which the nonlinear system is approximated by a linear system. The nonlinearities in (10) of the input–output normal-form are canceled by the linearizing feedback control law

$$\boldsymbol{u} = \boldsymbol{\beta}^{-1}(\boldsymbol{z})\big[\boldsymbol{v} - \boldsymbol{\alpha}(\boldsymbol{z})\big], \tag{12}$$

where $\boldsymbol{v}$ is a new input. It should be noted that this linearizing feedback law depends on all states $\boldsymbol{z}$ of the transformed system. Applying the linearizing feedback law (12) to the input–output normal-form (8)–(11), yields the partially linearized system

$$\boldsymbol{y} = \boldsymbol{z}_1 \tag{13}$$

$$\dot{\boldsymbol{z}}_1 = \boldsymbol{z}_2 \tag{14}$$

$$\dot{\boldsymbol{z}}_2 = \boldsymbol{v} \tag{15}$$

$$\dot{\boldsymbol{z}}_3 = \boldsymbol{\rho}(\boldsymbol{z}) + \boldsymbol{\sigma}(\boldsymbol{z})\,\boldsymbol{\beta}^{-1}(\boldsymbol{z})\big[\boldsymbol{v} - \boldsymbol{\alpha}(\boldsymbol{z})\big]. \tag{16}$$

Again, the system consists of two subsystems: Now the first subsystem describes the linear relationship between the new input $\boldsymbol{v}$ and the output $\boldsymbol{y}$, and consists of m chains of two integrators. Therefore, this approach is also called input–output linearization. The second subsystem (16) results from the internal dynamics and is in general nonlinear. From (14)–(16) it is seen that only the first subsystem influences the output. Thus the feedback law (12) renders the states $\boldsymbol{z}_3$ of the internal dynamics unobservable.

In this paper the control goal is trajectory tracking of a desired system output $\boldsymbol{y} = \boldsymbol{y}_d$. Following [7, 13] the new input $\boldsymbol{v}$ in (15) can be used in order to achieve asymptotic output trajectory tracking. The first subsystem is in canonical controllable form. Thus, linear control methods can be used to design a feedback controller, which influences the output $\boldsymbol{y}$ in a desired way with the new input $\boldsymbol{v}$. The investigated underactuated multibody systems have vector relative degree $r = \{2, \ldots, 2\}$ and therefore the tracking control law reads

$$\boldsymbol{v} = \ddot{\boldsymbol{y}}_d + \boldsymbol{p}_1(\dot{\boldsymbol{y}}_d - \dot{\boldsymbol{y}}) + \boldsymbol{p}_0(\boldsymbol{y}_d - \boldsymbol{y}). \tag{17}$$

Thereby, the coefficients $\boldsymbol{p}_0, \boldsymbol{p}_1$ are diagonal matrices. In the special case of a constant reference trajectory, $\boldsymbol{y} = \text{const}$, $\forall t$, the tracking control law (17) reduces to a control law for stabilization around a stationary point. Introducing the output trajectory error $\boldsymbol{e} = \boldsymbol{y}_d - \boldsymbol{y}$ and applying control law (17) to the linearized subsystem (14)–(15), yields the linear error dynamics

$$\ddot{\boldsymbol{e}} + \boldsymbol{p}_1\dot{\boldsymbol{e}} + \boldsymbol{p}_0\boldsymbol{e} = \boldsymbol{0}. \tag{18}$$

From this follows that the diagonal matrices $\boldsymbol{p}_0, \boldsymbol{p}_1$ can be used to place the eigenvalues of the error dynamics in the left half-plane. Then, due to a suitable choice of $\boldsymbol{p}_0, \boldsymbol{p}_1$ the system output $\boldsymbol{y}$ converges to the desired reference trajectory $\boldsymbol{y}_d$.

It should be noted that the linearizing state-feedback law (12) can be implemented in original coordinates $\boldsymbol{x}$ instead of $\boldsymbol{z}$ and reads in this case

$$\boldsymbol{u} = \boldsymbol{P}^{-1}\big(\boldsymbol{v} - \boldsymbol{H}\boldsymbol{M}^{-1}[\boldsymbol{g} - \boldsymbol{k}] - \bar{\boldsymbol{h}}\big). \tag{19}$$

The presented control structure is shown schematically in Fig. 1 and consists of an inner and an outer

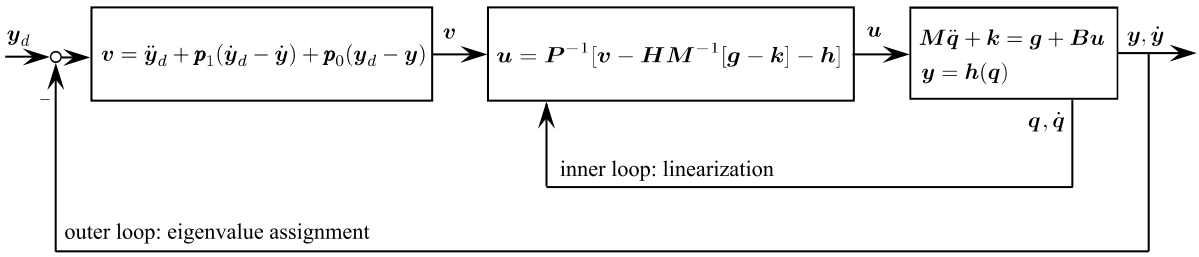

Fig. 1 Control structure with inner and outer loop for underactuated multibody system with vector relative degree $r = \{2, \ldots, 2\}$

loop. In the inner loop exact input–output linearization is achieved by using state-feedback law (19). The outer loop is used for eigenvalue assignment of the error dynamics (18) by control law (17). This is exactly the same control structure as using computed torque for fully actuated multibody systems. The only difference lies in the existence of the additional internal dynamics in the case of underactuation. The presented control structure requires full-state measurement. For multibody systems with passive joint this is easily realizable, using the direct measurement of unactuated generalized coordinates.

The task of controller design is not only to influence the output $\boldsymbol{y}$ in a desired way, but also to achieve that the whole dynamics of the system behaves well. Thus, the control design given by control law (17) can only be used, if the unobservable states z_3 of the internal dynamics remain bounded. Thus, a detailed investigation of the internal dynamics is necessary.

2.3 Analysis of the internal dynamics

The analysis of the behavior of the internal dynamics (11) is crucial for nonlinear control design. Since this analysis is often quite complex, the concept of zero dynamics is used to draw important conclusions about the boundedness of the states z_3 of the internal dynamics. The zero dynamics is the internal dynamics under the constraint that the output is kept constant or identical zero, i.e. $\boldsymbol{y} = \dot{\boldsymbol{y}} = \ddot{\boldsymbol{y}} = z_1 = z_2 = \dot{z}_2 = \boldsymbol{0},\ \forall t$. Thereby it is assumed that the new coordinates are chosen in such a way that $z^o = \boldsymbol{0}$ is an equilibrium point of the system. From (10) follows the required control input for this task as

$$\boldsymbol{u}_0 = -\boldsymbol{\beta}^{-1}(z)\,\boldsymbol{\alpha}(z) \quad \text{with } z = [\boldsymbol{0}, \boldsymbol{0}, z_3]^T. \tag{20}$$

Applying this input $\boldsymbol{u}_0$ to the internal dynamics (11) yields the zero dynamics of the system

$$\dot{z}_3 = \boldsymbol{\rho}(z) - \boldsymbol{\sigma}(z)\boldsymbol{\beta}^{-1}(z)\boldsymbol{\alpha}(z) \quad \text{with } z = [\boldsymbol{0}, \boldsymbol{0}, z_3]^T. \tag{21}$$

The zero dynamics is still a nonlinear system, however, it is time-invariant. Thus, in a first step local stability can be easily checked using Lyapunov's indirect method. Following [7, 13] a nonlinear system is called asymptotically (exponentially) minimum phase if the equilibrium point $z^o = \boldsymbol{0}$ of the zero dynamics is asymptotically (exponentially) stable. Otherwise, the system is called non-minimum phase. The minimum phase property is independent of the choice of coordinates, and thus is invariant under a diffeomorphic coordinate transformation $\boldsymbol{z} = \boldsymbol{\Phi}(\boldsymbol{x})$. However, the minimum phase property depends on the system dynamics given by the equation of motion (1) and the choice of the system output (2).

The internal dynamics (16) under the control law (17) can be viewed as a nonlinear time-varying system driven by the desired output trajectory $\boldsymbol{y}_d(t)$. In a first step the special case of tracking a constant output $\boldsymbol{y}_d = \text{const},\ \forall t$ is considered. In this case the tracking control law (17) coincides immediately with a stabilizing control law and leads to the requirement that the zero dynamics has to be asymptotically stable; i.e. the nonlinear system is minimum phase, see [7, 13, 22]. In the case of tracking a time-varying trajectory $\boldsymbol{y}_d(t)$, this is a necessary, but initially rather weak condition. However, from a practical point of view this is the crucial point for the analysis of the behavior of the internal dynamics. Then, additional conditions exist, which strengthen the requirement of minimum phase, see [7, 13, 22] for details. For example in [22] it is shown that for exponentially minimum phase nonlinear systems the desired trajectory $\boldsymbol{y}_d$ and its first $r_i - 1$

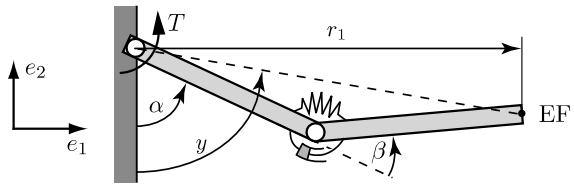

Fig. 2 Rotational arm with one active and one passive joint

derivatives must be small enough, in order to guarantee that control law (17) yields to convergence of the tracking error $\boldsymbol{e}$ and bounded internal states $\boldsymbol{z}_3$. In this paper these additional conditions are verified by simulation.

2.4 System with linearly combined output

The exact linearizing feedback law (19) can be implemented in original coordinates, and the complete coordinate transformation of the equation of motion is not necessary. However, for the analysis of the internal dynamics or feed-forward control design the explicit symbolic transformation is mostly necessary. For a general nonlinear output function $\boldsymbol{y} = \boldsymbol{h}(\boldsymbol{q})$, such as an end-effector position $\boldsymbol{r}^{\mathrm{ef}}(\boldsymbol{q})$, this is often not possible, since the symbolic solution of the nonlinear equation $\boldsymbol{y} = \boldsymbol{h}(\boldsymbol{q})$ might be necessary. Therefore, a simplified linearly combined system output is introduced, which yields a good approximation of the desired end-effector position of manipulators with passive joints. This output allows a symbolic transformation of the equation of motion into the nonlinear input–output normal-form. Therefore, it is assumed that the end-effector position can be approximately described by an output of form

$$\boldsymbol{y} = \boldsymbol{q}_a + \boldsymbol{\Gamma}\boldsymbol{q}_u, \tag{22}$$

where $\boldsymbol{\Gamma} \in \mathbb{R}^{m \times f-m}$. Thus, this output is a linear combination of actuated and unactuated generalized coordinates. Such an output cannot only be used to describe the end-effector position of manipulators with passive joints, as shown in this paper, but is also used for flexible manipulators as presented in [5, 18].

In the following the choice of such a linearly combined output is demonstrated exemplarily for a rotational arm with one passive joint. The arm consists of two links, connected by one active and one passive joint. The rotational arm is shown in Fig. 2, whereby the links have the length l_1, l_2. An input torque T acts on link 1. Link 2 is connected by a passive joint to link 1, which is supported by a spring-damper combination. The arm is described by the generalized coordinates $\boldsymbol{q} = [\alpha,\ \beta]^T$, whereby β denotes the unactuated coordinate. The control goal is tracking of the desired trajectory r_{1d} of the end-effector position $r_1(\boldsymbol{q})$ in e_1-direction. Assuming a stiff spring-damper combination, the β angle remains small. Then, $r_1(\boldsymbol{q})$ can be approximately described by the linearly combined output $y = \alpha + \Gamma\beta$ such that

$$\begin{aligned} r_1(\boldsymbol{q}) &= l_1 \sin(\alpha) + l_2 \sin(\alpha + \beta) \\ &\approx (l_1 + l_2)\sin(\alpha + \Gamma\beta) = (l_1 + l_2)\sin(y). \end{aligned} \tag{23}$$

Then, instead of tracking the position r_1, the output y can be tracked, which can be interpreted as an auxiliary angle to approximate the end-effector point. The desired trajectories y_d of the output can be computed from the desired trajectory r_{1d} and (23) using inverse kinematics. In order to determine the value Γ, a linearization around the nominal angles α_s and $\beta_s = 0$ is performed,

$$\begin{aligned} \Delta r_1 &= (l_1 + l_2)\cos(\alpha_s)\tilde{\alpha} + l_2 \cos(\alpha_s)\tilde{\beta} \\ &\approx (l_1 + l_2)\cos(\alpha_s)\tilde{\alpha} + (l_1 + l_2)\Gamma \cos(\alpha_s)\tilde{\beta}, \end{aligned} \tag{24}$$

where $\tilde{\alpha}, \tilde{\beta}$ are small deviations from the nominal angles. Thus, in the linearized case the output y describes exactly the position r_1 if $\Gamma = l_2/(l_1 + l_2)$. It should be noted that this relationship can also be derived using geometric considerations, see e.g. [18] for a flexible manipulator. Linearly combined outputs for manipulators with several passive joints are presented later in this paper for specific examples.

With such a special linearly combined system output (22), the nonlinear input–output normal-form can be directly derived from the partitioned equation of motion (3). The coordinate transformation $\boldsymbol{z} = \boldsymbol{\Phi}(\boldsymbol{x})$ is given by

$$\boldsymbol{z} = \begin{bmatrix} \boldsymbol{y} \\ \dot{\boldsymbol{y}} \\ \boldsymbol{q}_u \\ \dot{\boldsymbol{q}}_u \end{bmatrix} = \begin{bmatrix} \boldsymbol{q}_a + \boldsymbol{\Gamma}\boldsymbol{q}_u \\ \dot{\boldsymbol{q}}_a + \boldsymbol{\Gamma}\dot{\boldsymbol{q}}_u \\ \boldsymbol{q}_u \\ \dot{\boldsymbol{q}}_u \end{bmatrix}. \tag{25}$$

This forms a local diffeomorphic coordinate transformation. In order to derive the input–output normal-form, the starting point is the expression of the actuated coordinates $\boldsymbol{q}_a$ in terms of the output $\boldsymbol{y}$ and

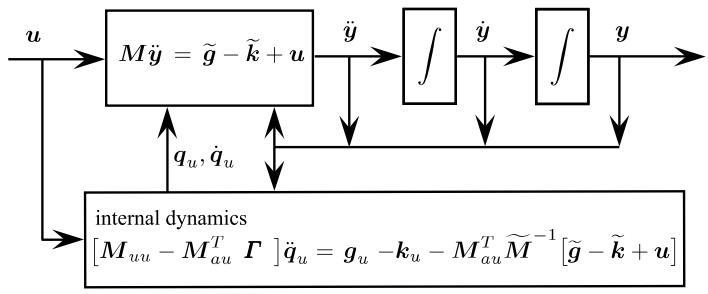

Fig. 3 Graphical representation of the input–output normal-form of underactuated MBS with linearly combined output

the unactuated coordinates $\boldsymbol{q}_u$, i.e. $\boldsymbol{q}_a = \boldsymbol{y} - \boldsymbol{\Gamma}\boldsymbol{q}_u$, $\dot{\boldsymbol{q}}_a = \dot{\boldsymbol{y}} - \boldsymbol{\Gamma}\dot{\boldsymbol{q}}_u$ and $\ddot{\boldsymbol{q}}_a = \ddot{\boldsymbol{y}} - \boldsymbol{\Gamma}\ddot{\boldsymbol{q}}_u$. Then, these expressions can be used in the equation of motion (3). Note that the actuated coordinates $\boldsymbol{q}_a$ are also replaced in all the entries of $\boldsymbol{M}$, $\boldsymbol{k}$ and $\boldsymbol{g}$. For reasons of readability these dependencies are dropped in most of the following calculations. From the unactuated part of the differential equation (3) an expression for $\ddot{\boldsymbol{q}}_u$ can be obtained as

$$\ddot{\boldsymbol{q}}_u = \big(\boldsymbol{M}_{uu} - \boldsymbol{M}_{au}^T\boldsymbol{\Gamma}\big)^{-1}\big(\boldsymbol{g}_u - \boldsymbol{k}_u - \boldsymbol{M}_{au}^T\ddot{\boldsymbol{y}}\big). \tag{26}$$

Inserting (26) in the actuated part of (3) and reordering yields

$$\widetilde{\boldsymbol{M}}(\boldsymbol{y}, \boldsymbol{q}_u)\ddot{\boldsymbol{y}} = \widetilde{\boldsymbol{g}}(\boldsymbol{y}, \dot{\boldsymbol{y}}, \boldsymbol{q}_u, \dot{\boldsymbol{q}}_u) - \widetilde{\boldsymbol{k}}(\boldsymbol{y}, \dot{\boldsymbol{y}}, \boldsymbol{q}_u, \dot{\boldsymbol{q}}_u) + \boldsymbol{u}, \tag{27}$$

where the terms are summarized according to the convention

$$\widetilde{\boldsymbol{M}} = \boldsymbol{M}_{aa} - (\boldsymbol{M}_{au} - \boldsymbol{M}_{aa}\boldsymbol{\Gamma})\big(\boldsymbol{M}_{uu} - \boldsymbol{M}_{au}^T\boldsymbol{\Gamma}\big)^{-1}\boldsymbol{M}_{au}^T,$$
$$\widetilde{\boldsymbol{g}} = \boldsymbol{g}_a - (\boldsymbol{M}_{au} - \boldsymbol{M}_{aa}\boldsymbol{\Gamma})\big(\boldsymbol{M}_{uu} - \boldsymbol{M}_{au}^T\boldsymbol{\Gamma}\big)^{-1}\boldsymbol{g}_u,$$
$$\widetilde{\boldsymbol{k}} = \boldsymbol{k}_a - (\boldsymbol{M}_{au} - \boldsymbol{M}_{aa}\boldsymbol{\Gamma})\big(\boldsymbol{M}_{uu} - \boldsymbol{M}_{au}^T\boldsymbol{\Gamma}\big)^{-1}\boldsymbol{k}_u.$$

Solving (27) for $\ddot{\boldsymbol{y}}$ and inserting in (26) yields a differential equation for $\ddot{\boldsymbol{q}}_u$. Summarizing these calculations yields the nonlinear input–output normal-form

$$\widetilde{\boldsymbol{M}}\ddot{\boldsymbol{y}} = \widetilde{\boldsymbol{g}} - \widetilde{\boldsymbol{k}} + \boldsymbol{u}, \tag{28}$$

$$\big[\boldsymbol{M}_{uu} - \boldsymbol{M}_{au}^T\boldsymbol{\Gamma}\big]\ddot{\boldsymbol{q}}_u = \boldsymbol{g}_u - \boldsymbol{k}_u - \boldsymbol{M}_{au}^T\widetilde{\boldsymbol{M}}^{-1}\big[\widetilde{\boldsymbol{g}} - \widetilde{\boldsymbol{k}} + \boldsymbol{u}\big]. \tag{29}$$

Equation (28) is a second-order differential equation of dimension m and describes the relationship between the input $\boldsymbol{u}$ and output $\boldsymbol{y}$, corresponding to (9)–(10). The second part of the normal-form, given by (29), has dimension $f - m$ and describes the internal dynamics and corresponds to (11). A graphical representation of the nonlinear input–output normal-form of an underactuated multibody system with the linearly combined system output (22) is shown in Fig. 3.

Finally, for underactuated multibody systems with linearly combined output, the zero dynamics can be simply derived in symbolic form from the input–output normal-form (28)–(29) by setting $\boldsymbol{y} = \dot{\boldsymbol{y}} = \ddot{\boldsymbol{y}} = \boldsymbol{0}$, $\forall t$. Thus, the required control input for keeping the output constant zero follows from (28) as

$$\boldsymbol{u}_0 = \widetilde{\boldsymbol{k}}(\boldsymbol{0}, \boldsymbol{0}, \boldsymbol{q}_u, \dot{\boldsymbol{q}}_u) - \widetilde{\boldsymbol{g}}(\boldsymbol{0}, \boldsymbol{0}, \boldsymbol{q}_u, \dot{\boldsymbol{q}}_u). \tag{30}$$

With this input $\boldsymbol{u}_0$ the internal dynamics (29) reduces to the zero dynamics

$$\big[\boldsymbol{M}_{uu}(\boldsymbol{0}, \boldsymbol{q}_u) - \boldsymbol{M}_{au}^T(\boldsymbol{0}, \boldsymbol{q}_u)\boldsymbol{\Gamma}\big]\ddot{\boldsymbol{q}}_u = \boldsymbol{g}_u(\boldsymbol{0}, \boldsymbol{0}, \boldsymbol{q}_u, \dot{\boldsymbol{q}}_u) - \boldsymbol{k}_u(\boldsymbol{0}, \boldsymbol{0}, \boldsymbol{q}_u, \dot{\boldsymbol{q}}_u). \tag{31}$$

This zero dynamics is symbolically available for the stability investigations and is also used in the next section for the optimization of the system. In the following the Jacobian linearization of the zero dynamics (31) in state space is denoted by $\dot{\tilde{\boldsymbol{z}}} = \boldsymbol{A}\tilde{\boldsymbol{z}}$, where $\boldsymbol{A}$ is the system matrix.

2.5 A note on feed-forward control design

The use of feedback linearization might have several drawbacks. For example, full-state information is necessary which is not always available, e.g. the elastic coordinates in flexible multibody systems. Also, due to parameter uncertainty robustness issues might arise. Thus, alternatively to feedback linearization a control structure consisting of a feed-forward control and an additional feedback controller to account for small disturbances and uncertainties might be used. The feed-forward control design is based on an inverse model

which provides the input $\boldsymbol{u}_d$ required for exact reproduction of the desired output trajectory $\boldsymbol{y}_d$. The inverse model can be directly derived from the input–output normal-form; see e.g. [13]. Here it is presented for a linearly combined output. The input $\boldsymbol{u}_d$ computed by the feed-forward control follows from (28) as

$$\boldsymbol{u}_d = \widetilde{\boldsymbol{M}}(\boldsymbol{y}_d, \boldsymbol{q}_u)\ddot{\boldsymbol{y}}_d - \widetilde{\boldsymbol{g}}(\boldsymbol{y}_d, \boldsymbol{q}_u, \dot{\boldsymbol{y}}_d, \dot{\boldsymbol{q}}_u) + \widetilde{\boldsymbol{k}}(\boldsymbol{y}_d, \boldsymbol{q}_u, \dot{\boldsymbol{y}}_d, \dot{\boldsymbol{q}}_u). \tag{32}$$

The computation of the input $\boldsymbol{u}_d$ depends on the desired output trajectory $\boldsymbol{y}_d$, $\dot{\boldsymbol{y}}_d$ and the unactuated states $\boldsymbol{q}_u, \dot{\boldsymbol{q}}_u$. These latter ones are the solution of the internal dynamics (29), which is driven by $\boldsymbol{y}_d$, $\dot{\boldsymbol{y}}_d$ and $\boldsymbol{u}_d$. Replacing $\boldsymbol{u}_d$ in the internal dynamics (29) by (32) yields for the unactuated states $\boldsymbol{q}_u, \dot{\boldsymbol{q}}_u$ the differential equation

$$\left[\boldsymbol{M}_{uu} - \boldsymbol{M}_{au}^T \boldsymbol{\Gamma}\right]\ddot{\boldsymbol{q}}_u = \boldsymbol{g}_u - \boldsymbol{k}_u - \boldsymbol{M}_{au}^T \ddot{\boldsymbol{y}}_d. \tag{33}$$

Thus, the inverse model consists of three parts: a chain of two differentiators for the desired output vector $\boldsymbol{y}_d$ producing the values $\dot{\boldsymbol{y}}_d$ and $\ddot{\boldsymbol{y}}_d$, the driven internal dynamics (33) for the $\boldsymbol{q}_u, \dot{\boldsymbol{q}}_u$ coordinates and the algebraic equation (32), which computes from these values the desired input $\boldsymbol{u}_d$. A solution for the driven internal dynamics (33) must be determined. This can only be computed by forward time integration if the $\boldsymbol{q}_u, \dot{\boldsymbol{q}}_u$ states of the internal dynamics remain bounded, which implies that the system must be minimum phase. Otherwise unbounded states $\boldsymbol{q}_u, \dot{\boldsymbol{q}}_u$ occur. For non-minimum phase systems a bounded solution for the states $\boldsymbol{q}_u, \dot{\boldsymbol{q}}_u$ can be computed in the feed-forward control by solving a two-sided boundary value problem, see [6, 20, 24] for details. However, this is often a non-trivial challenging task and yields a non-causal feed-forward control. Therefore, also in the feed-forward control design a minimum phase system is desired.

3 Design of stable zero dynamics

As discussed in the previous section, feedback linearizable is only possible if the system is minimum phase. Also in this case the design of feed-forward control is significantly simplified. However, the analysis of the initial design of an underactuated multibody system might show that it possess unstable zero dynamics; and is therefore non-minimum phase. Thus, it is desired to design the multibody system in such a way that the zero dynamics is stable. As shown in Sect. 2.3, the zero dynamics depends on the choice of the system output $\boldsymbol{y}$ and the equation of motion (1) of the multibody system. Output relocation is a method where a different system output $\hat{\boldsymbol{y}}$ is chosen in order to achieve minimum phase property. An analysis of this approach for a flexible two-arm manipulator is given in [12]. However, the use of this approach is limited in trajectory tracking of an end-effector point, since the relocated output normally does not approximate the desired output well. Thus, minimum phase property can only be achieved by modifying the system dynamics, which means the mechanical design of the underactuated multibody system must be altered.

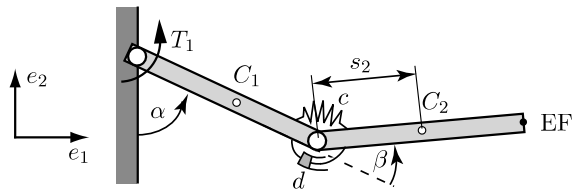

Fig. 4 Rotational arm with one active and one passive joint

3.1 Identification of possible design parameters

In a first step possible physical design parameters which influence the stability properties of the zero dynamics are identified. For this task the explicit symbolically derived input–output normal-form (28)–(29) and the resulting zero dynamics (31) are used. The investigation is performed exemplarily for a single rotational arm with a passive joint, which is presented in Fig. 4. The arm consist of two links $i = 1, 2$, whose center of mass is denoted by C_i. The links have length l_i, mass m_i, inertia I_{iz} and the position of the center of mass is described by s_i. Link 2 is connected by a passive joint to link 1, which is supported by a spring-damper combination with spring constant c and damping coefficient d. The arm is described by the generalized coordinates α and β, whereby β denotes the unactuated coordinate. The arm moves in the horizontal plane perpendicular to the direction of gravity.

As described in Sect. 2.4 the end-effector point can be described approximately by the linear combined system output $y = \alpha + \Gamma\beta$ with $\Gamma = l_2/(l_1 + l_2)$. In

this case the zero dynamics of the rotational arm is

$$\left[\frac{l_1(I_{2z}+m_2s_2^2)-l_1l_2m_2s_2}{l_1+l_2}\cos\beta\right]\ddot{\beta} = -c\beta - d\dot{\beta} - \frac{l_1l_2^2m_2s_2}{(l_1+l_2)^2}\dot{\beta}^2\sin\beta.$$

This shows that the zero dynamics of the rotational arm is influenced by the length l_1, l_2 of both links, mass m_2, inertia I_{2z} and center of mass s_2 of the second link as well as the coefficients c, d of the spring-damper combination. For a further analysis the linearized zero dynamics around the equilibrium point $\beta = 0$ is considered,

$$\left[\frac{l_1(I_{2z}+m_2s_2^2)-l_1l_2m_2s_2}{l_1+l_2}\right]\ddot{\tilde{\beta}} + d\dot{\tilde{\beta}} + c\tilde{\beta} = a_2\ddot{\tilde{\beta}} + a_1\dot{\tilde{\beta}} + a_0\tilde{\beta} = 0, \tag{34}$$

where a_2, a_1, a_0 correspond to the coefficients of the characteristic polynomial. Thus, the linearized zero dynamics of the rotational arm is only asymptotically stable, if all coefficients a_2, a_1, a_0 have the same sign and are non-zero. Since the constants c, d of the spring-damper combination are by nature positive also the coefficient a_2 has to be positive. Thus, in this case c, d can only be used to shape the dynamic response of the zero dynamics, but cannot be used to change its stability property. However, the stability property of the zero dynamics can be influenced by changing the mass distribution of the second link, which is given by the mass m_2, inertia I_{2z} and center of mass s_2. In addition a change of the geometry, i.e. length of the links l_1, l_2, can be used to alter the stability property. This analysis, which shows the influence of the mass distribution and geometry on the stability of the zero dynamics, is representative for all underactuated multibody systems considered in this paper.

The mass distribution of the unactuated link and the geometry of both links could be used here directly as design variables,

$$\boldsymbol{p} = [m_2,\ I_{2z},\ s_2,\ l_1,\ l_2]. \tag{35}$$

However, these quantities are highly coupled, and an optimization-based design procedure might yield values which cannot be realized from an engineering point of view. Therefore, more sophisticated parameterizations of the design variables are necessary.

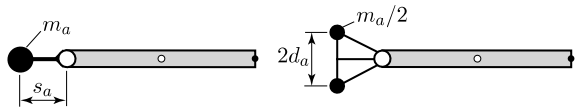

Fig. 5 Two possible design variants for altering the mass distribution of a link

In this paper different design parameterization approaches are used to alter the mass distribution and geometry. Thereby, in all approaches it turns out that the change of the center of mass of the links is crucial. The basic approach proposed here, is based on the introduction of additional small balancing weights. Assuming the geometry is fixed, the mass distribution of an initially homogeneous design is altered by adding a small mass m_a to the unactuated link. The additional mass is added at the location s_a, which changes the center of mass of the combined body. An additional increase of the inertia I_{2z} of the unactuated link can be achieved, if the mass m_a is located by an offset d_a away from the axis of the link. Two possible design variants for an unactuated link are shown schematically in Fig. 5, whereby the additional mass is mounted as counterweight. Neglecting for simplicity the weight of the mounting rods, the three design variables $\boldsymbol{p} = [m_a, s_a, d_a]$ can be used to alter the mass distribution of an unactuated link and yield

$$m_2 = \bar{m}_2 + m_a, \qquad s_2 = \frac{\bar{m}_2\bar{s}_2 + m_a s_a}{m_2},$$
$$I_{2z} = \bar{I}_{2z} + \bar{m}_2(\bar{s}_2 - s_2)^2 + m_a(s_a - s_2)^2 + m_a d_a^2.$$

Thereby $\bar{m}_2, \bar{I}_{2z}, \bar{s}_2$ denote the values of the initial design of the unactuated link. In order to obtain a viable physical design, bounds have to be put on the design variables which results in the feasible design space for one unactuated link

$$P = \big\{\boldsymbol{p} \in \mathbb{R}^3 | 0 \le m_a \le m_{a_{\max}},\ s_{a_{\min}} \le s_a \le s_{a_{\max}}, 0 \le d_a \le d_{a_{\max}}\big\}.$$

For underactuated multibody systems with several passive joints, the design variables $\boldsymbol{p}$ and the feasible design space P are the collection of the design variables of all links whose mass distribution should be altered. This basic parameterization can be further modified, e.g. by adding the link length to the design variables or by constraining the total mass of the multibody system. Detailed description on these

further reaching approaches are presented later in the paper for specific examples.

3.2 Optimization criteria

For the minimum phase design of underactuated multibody systems an optimization-based design procedure is proposed, using the previously identified design parameters $\boldsymbol{p}$. The zero dynamics (31) depends only on the unactuated states $\boldsymbol{q}_u, \dot{\boldsymbol{q}}_u$ and the design variables $\boldsymbol{p}$. Therefore, the zero dynamics is given by

$$\begin{aligned}&\left[\boldsymbol{M}_{uu}(\boldsymbol{p},\boldsymbol{q}_u)-\boldsymbol{M}_{au}^T(\boldsymbol{p},\boldsymbol{q}_u)\boldsymbol{\Gamma}\right]\ddot{\boldsymbol{q}}_u\\&\quad=\boldsymbol{g}_u(\boldsymbol{p},\boldsymbol{q}_u,\dot{\boldsymbol{q}}_u)-\boldsymbol{k}_u(\boldsymbol{p},\boldsymbol{q}_u,\dot{\boldsymbol{q}}_u).\end{aligned}\tag{36}$$

In the following the system matrix of the linearized zero dynamics (36) is denoted by $\boldsymbol{A}(\boldsymbol{p})$.

The primary design goal is to achieve a stable zero dynamics, such that the underactuated multibody system is feedback linearizable. However, in order to obtain a powerful mechanical design, not only minimum phase behavior must be guaranteed, but also disturbances in the zero dynamics should decay rapidly. This is especially important in order to avoid that disturbances yield large undesired vibrations of the internal dynamics during trajectory tracking. Therefore, a two-step computation of the optimization criteria $f(\boldsymbol{p})$ is proposed, which should be minimized in the course of the optimization. The two steps of the optimization criteria computation are as follows.

Step 1: Firstly, Lyapunov's indirect method is used, see [10]. It requires that all eigenvalues of the linearized zero dynamics are in the left half-plane,

$$\mathrm{Re}\left[\lambda\left(\boldsymbol{A}(\boldsymbol{p})\right)\right]<0.\tag{37}$$

If at least one eigenvalue has a non-negative real part, a large default value for the optimization criteria $f(\boldsymbol{p})$ is returned. Otherwise, the linearized analysis shows asymptotic stability and the optimization can be proceeded with step 2.

Step 2: If all eigenvalues are in the left half-plane, the final optimization criteria $f(\boldsymbol{p})$ is calculated. In order to achieve good damping properties, it is required that initial errors in the nonlinear zero dynamics (36) decay rapidly. The disturbance is given by the initial conditions $\boldsymbol{q}_u(t_0)=\boldsymbol{q}_{u_0}, \dot{\boldsymbol{q}}_u(t_0)=\dot{\boldsymbol{q}}_{u_0}$. The damping property is then described by the integrated error of the unactuated coordinates $\boldsymbol{q}_u$ in respect to the equilibrium point $\boldsymbol{q}_u=\boldsymbol{0}$ of the zero dynamics. Thereby, the optimization criteria is chosen as the maximum of the integrated error of the $f-m$ unactuated coordinates $\boldsymbol{q}_u$. This is given by

$$f(\boldsymbol{p})=\max_i\int_{t_0}^{t_1}q_{u_i}^2\,dt,\tag{38}$$

where t_1 describes the final time of the simulation. By evaluating only the attenuation of the least damped coordinate of the zero dynamics, it is achieved that improvements in the other coordinates with better damping properties are ignored. Thus, the design procedure concentrates on the improvement of the damping properties of the least damped coordinate.

Besides evaluating the damping properties of the zero dynamics, the second step provides also a very good indication about the behavior of the nonlinear zero dynamics. By choosing large initial conditions, it can be checked, if the nonlinear zero dynamics remains bounded in the case that their states $\boldsymbol{q}_u\,\dot{\boldsymbol{q}}_u$ are pushed by a disturbance further away from the equilibrium point. If this is not the case, the states $\boldsymbol{q}_u\,\dot{\boldsymbol{q}}_u$ become unbounded and the integration fails. Then, also a large default value is returned for the optimization criteria $f(\boldsymbol{p})$.

In the criteria computation the most time consuming part is the time integration of the zero dynamics in the second step. However, in the first step of the criteria computation many unfeasible designs are filtered out; thus the number of time integrations is reduced by the restriction on locally stable designs.

Also the first step can be efficiently used to achieve further design goals, such as robustness to uncertainties in the mass distribution. This means that the system should remain its minimum phase property even if there are some small unknown variations in the physical construction. These uncertainties can be either in the initial mass distribution or in the optimal design variables. Thus, for example in the first step, it can also be desired that the eigenvalues for several perturbation parameter sets $\boldsymbol{p}+\Delta\boldsymbol{p}$ are in the left half-plane and (37) is supplemented by,

$$\mathrm{Re}\left[\lambda\left(\boldsymbol{A}(\boldsymbol{p}+\Delta\boldsymbol{p})\right)\right]<0.\tag{39}$$

In this paper up to 16 designs with perturbation are tested, whereby the design parameters are varied in different combination by up to 5% around the nominal values $\boldsymbol{p}$. By this approach, also some nominal designs are filtered out which are close to an unstable region

and yield unbounded states of the zero dynamics in the following time integration. It should be noted that here only a point-wise robustness test is performed, which does not guarantee robustness over the entire region of uncertainties. In order to achieve this, the point-wise test can be replaced by a μ-analysis, see e.g. [21] for details on analysis of system robustness. However, this is computationally much more time consuming. In numerical tests of the proposed optimization procedure it turns out that the combination of the point-wise test with the simulation of the nonlinear zero dynamics is sufficient to obtain a robust mechanical design with good damping properties in a time efficient way.

3.3 Particle swarm optimization

In the optimization procedure the criteria function $f(\boldsymbol{p})$ should be minimized with respect to the design variables $\boldsymbol{p}$,

$$\min_{\boldsymbol{p}\in P} f(\boldsymbol{p}). \tag{40}$$

Due to the two-step criteria computation, the optimization problem is discontinuous. Also, an analysis of this optimization problem shows that there are many local minima and the complexity of the optimization criteria increases with the number of passive joints. Therefore, gradient-based optimization algorithms cannot be used and stochastic optimization algorithms must be deployed. Here a particle swarm optimization procedure is used. This is a population-based optimization method which originates in the study and simulation of social behavior of bird and fish flocks, see [8]. The basic idea is the modeling of social interaction between individual particles of a population on the quest for the best point in the feasible design space. Thereby, it is aspired to use the collective intelligence of a swarm to solve complex optimization problems. A detailed analysis of swarm intelligence is given in [9].

The basic step of the particle swarm optimization is the recursive update equation to compute the new parameter set $\boldsymbol{p}_i$ of the i-th particle of the swarm

$$\begin{aligned}\boldsymbol{p}_i^{k+1} &= \boldsymbol{p}_i^k + \Delta\boldsymbol{p}_i^{k+1}\\ \Delta\boldsymbol{p}_i^{k+1} &= w\Delta\boldsymbol{p}_i^k + c_1 r_1\big(\boldsymbol{p}_i^{\text{best},k} - \boldsymbol{p}_i^k\big)\\ &\quad + c_2 r_1\big(\boldsymbol{p}_{\text{swarm}}^{\text{best},k} - \boldsymbol{p}_i^k\big).\end{aligned} \tag{41}$$

Thereby, k is the number of iterations and r_1, r_2 are evenly distributed numbers. The update of the particle's parameters $\Delta\boldsymbol{p}_i^{k+1}$ consist of three contributions. The first contribution describes the tradition and the particle moves in the direction of the previous update $\Delta\boldsymbol{p}_i^k$. The second part describes the cognitive part and the particle moves in the direction of the best parameter set $\boldsymbol{p}_i^{\text{best},k}$, which it found on its own. The third part describes the social behavior, and the particle moves in the direction of the best parameter set $\boldsymbol{p}_{\text{swarm}}^{\text{best},k}$, which the entire swarm has found so far. With the three parameters w, c_1, c_2 the contributions are weighted, and the convergence speed and the width of the search can be controlled.

An advantage of the particle swarm optimization is that no gradient information is necessary, the solution is independent of initial sets of design parameters $\boldsymbol{p}$ and there are no requirements on smoothness or continuity of the optimization criteria. This approach is well suited for finding global minima and is often easy to program and to adjust to specific problems. The used algorithm is a Matlab implementation presented in [14, 15] and has been already successfully applied in the optimization of multibody systems. Compared to gradient-based methods, a general disadvantage of stochastic optimization algorithms is their large computational expense due to a large amount of criteria evaluations. However, due to the two-step criteria computation, the number of time intensive time integrations is limited.

4 Examples

In this section the efficiency of the optimization-based design approach for underactuated multibody systems is demonstrated. Four examples are presented, which are the design of planar manipulators with two and four passive joints, respectively, and a kinematic redundancy. Three different parameterizations for the design variables are presented. Corresponding results for a manipulator with one passive joint are presented in [16, 17]. In the first example the advantages of the presented integrated optimization-based design and control approach are compared to other possible control strategies. The second and third example show two different design parameterizations which can be used to obtain a viable minimum phase design, while keeping the mass of the system constant. In the forth example the design for a larger system is presented, and its robustness against uncertainty is demonstrated by simulation.

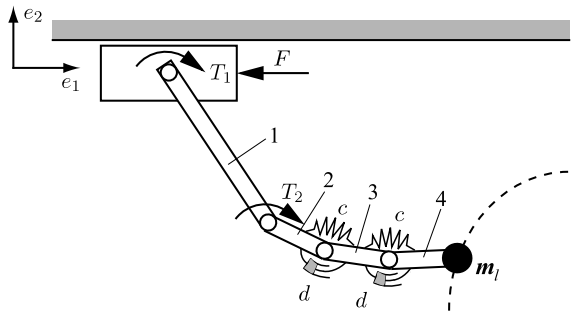

Fig. 6 Underactuated manipulator with two passive joints

Table 1 Initial parameters for underactuated manipulator with two passive joints

Cart	$m_c = 3$ kg		
Link 1	$m_1 = 6.875$ kg	$I_1 = 0.5743$ kgm^2	$l_1 = 1.0$ m
Link $i = 2, 3, 4$	$m_i = 2.292$ kg	$I_i = 0.0217$ kgm^2	$l_i = 1/3$ m
Load	$m_l = 6$ kg	$I_l = 0.0147$ kgm^2	
	$c = 400\ \frac{\text{Nm}}{\text{rad}}$	$d = 0.25\ \frac{\text{Nms}}{\text{rad}}$	

4.1 Manipulator with two passive joints: change of mass distribution

The first investigated manipulator is shown schematically in Fig. 6. The manipulator moves along the horizontal plane and consists of a cart on which a chain of four links is mounted. The homogeneous links have length l_1 and $l_2 = l_3 = l_3$ and squared cross section with width 50 mm. At the end-effector point an additional load is applied. The actuated generalized coordinates are $\boldsymbol{q}_a = [x, \alpha_1, \alpha_2]^T$ and the unactuated generalized coordinates are $\boldsymbol{q}_u = [\beta_1, \beta_2]^T$. These are defined as relative joint coordinates. Thereby β_1 is the angle between link 2 and 3, β_2 is the angle between link 3 and 4. The manipulator is actuated by the control input $\boldsymbol{u} = [F, T_1, T_2]^T$. The system output is the cart position and the end-effector position,

$$\boldsymbol{y} = \boldsymbol{h}(\boldsymbol{q}) = \begin{bmatrix} x \\ \boldsymbol{r}^{\text{ef}}(\boldsymbol{q}) \end{bmatrix}. \tag{42}$$

The passive joints are supported by parallel spring-damper combinations with spring constant c and damping coefficient d. The physical properties are summarized in Table 1.

For the analysis of the zero dynamics and the optimization the approximation of the end-effector position

$$\begin{aligned} &\boldsymbol{r}^{\text{ef}}(\boldsymbol{q}_a, \boldsymbol{q}_u) \\ &\quad \approx \boldsymbol{r}^{\text{ef}}(\boldsymbol{y}) \\ &\quad = \begin{bmatrix} y_1 + l_1 \sin(y_2) + (l_2 + l_3 + l_4)\sin(y_2 + y_3) \\ -l_1 \cos(y_2) - (l_2 + l_3 + l_3)\cos(y_2 + y_3) \end{bmatrix}, \end{aligned} \tag{43}$$

is used. Thereby, similar to Sect. 2.4, a linearly combined system output $\boldsymbol{y}$ is chosen as

$$\boldsymbol{y} = \boldsymbol{q}_a + \boldsymbol{\Gamma}\boldsymbol{q}_u \quad \text{with } \boldsymbol{\Gamma} = \begin{bmatrix} 0 & 0 \\ 0 & 0 \\ \Gamma_1 & \Gamma_2 \end{bmatrix}. \tag{44}$$

In this example a good approximation is achieved for $\Gamma_1 = (l_3 + l_4)/(l_2 + l_3 + l_4) = 2/3$ and $\Gamma_2 = l_4/(l_2 + l_3 + l_4) = 1/3$. As described in Sect. 2.4 the angle $y_3 = \alpha_2 + \Gamma_1\beta_1 + \Gamma_2\beta_2$ can be viewed as an auxiliary angle to approximate the end-effector position, if β_1, β_2 remain small. Using $\boldsymbol{y}$ as system output, their desired trajectories can be computed from the desired trajectory $\boldsymbol{r}_d^{\text{ef}}$ and (43) by inverse kinematics.

The analysis of the manipulator shows that the initial design is non-minimum phase. Thus the proposed optimization procedure is used to alter the initial design in order to achieve a minimum phase manipulator. The analysis of the zero-dynamics shows that its stability depends on the mass distribution of the unactuated links 3 and 4. Following Sect. 3.1, the mass distribution is altered by adding additional masses to these two links. This represents the case of an already existing machine, where additional mass can be added, but existing weight cannot be removed any more. Thus, six design variables are introduced

$$\boldsymbol{p} = [m_{a_3},\ s_{a_3},\ d_{a_3},\ m_{a_4},\ s_{a_4},\ d_{a_4}], \tag{45}$$

describing the additional masses m_{a_3}, m_{a_4}, their positions s_{a_3}, s_{a_4} along the link axis and the offset variable d_{a_3}, d_{a_4} for link 3 and 4, respectively. Thereby, a negative value for s_{a_i} indicates that the additional mass is added as counterweight to link i. Since this manipulator moves in the horizontal plane, there are infinity equilibrium points. In this considered example, the zero-dynamics is identical for all these equilibrium points. An analysis of the zero dynamics of this manipulator shows that many designs with similar criteria values exist and the influence of the mass

Table 2 Example 1—bounds and optimization results

link 3	m_{a_3} [kg]	s_{a_3} [m]	d_{a_3} [m]
Lower bound	0	−0.333	0
Upper bound	1	0.333	0.167
Optimization result	0.999	−0.293	0.062
link 4	m_{a_4} [kg]	s_{a_4} [m]	d_{a_4} [m]
Lower bound	0	−0.333	0
Upper bound	2	0.333	0.167
Optimization result	1.997	−0.333	0.166

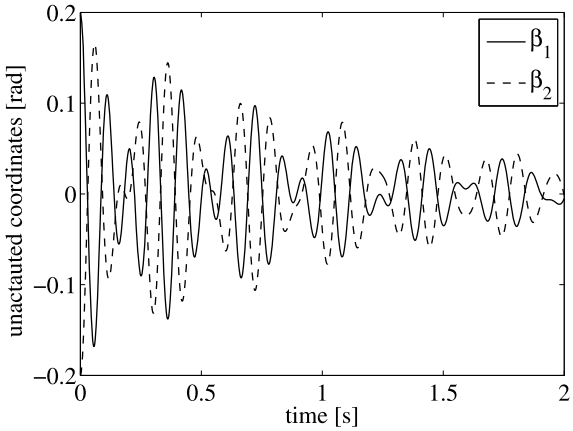

Fig. 7 Attenuation of the zero dynamics of example 1 under initial disturbance

distribution of the two unactuated arms on the zero dynamics is coupled.

Table 2 shows the bounds on the parameters and the obtained optimization result. Thereby, the particle swarm optimization uses 100 particles and 22 iterations are performed. The optimization procedure is implemented in Matlab, and it takes only approximately 240 s. In Fig. 7 the attenuation of an initial disturbance in the unactuated coordinates β_1, β_2 of the zero dynamics is shown. Both coordinates have a relatively even attenuation behavior. This is achieved by the optimization criteria (38), which concentrates on increasing the damping properties of the least damped unactuated coordinate of the zero dynamics. This example shows that the presented approach is a very time efficient method to design minimum phase underactuated multibody systems with good damping properties. For verification purpose the optimization is performed several times. These show very similar designs, whereby

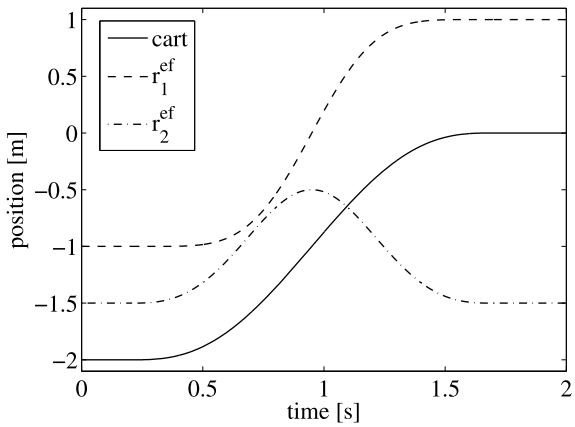

Fig. 8 Desired trajectory of end-effector and cart

only some variations in the d_{a_3} variables are observed. However, the function value f are nearly identical, indicating local minima. It is worth to notice that the additional masses are always placed as counterweights. It should be noted that the offset d_{a_i} is not necessary to find a minimum phase design, however, it allows to use smaller additional masses, see [16, 17] for details.

The obtained optimal designs are tested by simulation considering a half-circular end-effector trajectory. The center of the half-circle is at position $(0, -1.5\ \text{m})$ and the radius is 1 m. The end-effector point should follow the trajectory in the short time period of 1.5 s, which describes an aggressive maneuver. Also the kinematic redundancy should be used to perform a secondary task, which is moving the cart from starting position −2 m to the final position 0 m. The motion starts at time 0.2 s and ends at time 1.7 s. The desired trajectories are shown in Fig. 8.

In the simulation the described feedback linearization controller is applied to the obtained optimized design. Thereby, the exact end-effector point $\boldsymbol{r}^{\text{ef}}(\boldsymbol{q}_a, \boldsymbol{q}_u)$ is used, as well as the approximated point $\boldsymbol{r}^{\text{ef}}(\boldsymbol{y})$, which is used in the optimization. These results are compared to those using two alternative control concepts, which are applied to the initial design of the manipulator. The first alternative control approach is a feedback linearization, whereby minimum phase property of the initial system is achieved by output relocation. An analysis of the zero dynamics shows that in this example output relocation with $\Gamma_1 = 0.570$ and $\Gamma_2 = 0.333$ yields a minimum phase design. The second approach is a stable inversion-based feed-forward control of the non-minimum phase initial system com-

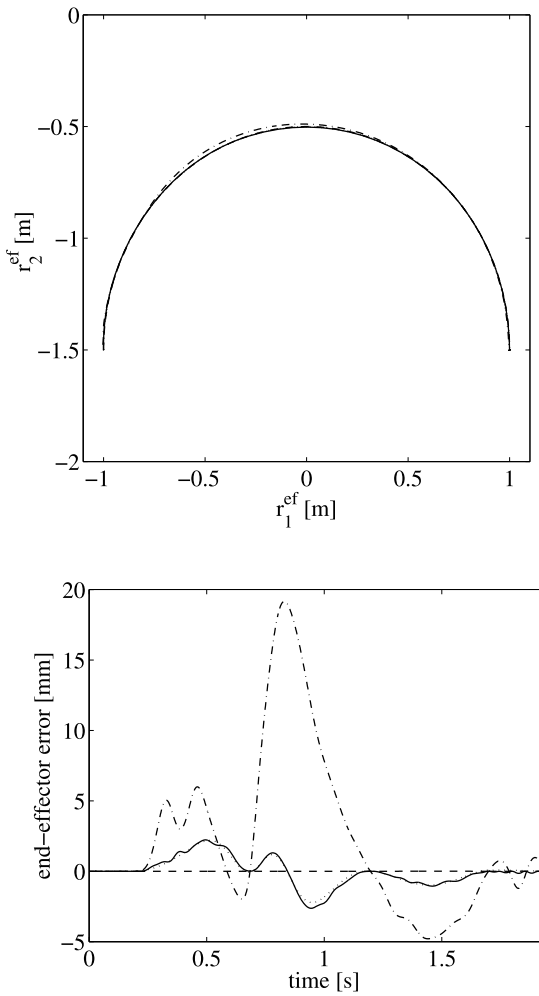

Fig. 9 Trajectory (*top*) and error in radial direction (*bottom*) of end-effector (— optimized design with $\boldsymbol{r}^{\mathrm{ef}}(\boldsymbol{y})$; – – optimized design with $\boldsymbol{r}^{\mathrm{ef}}(\boldsymbol{q}_a, \boldsymbol{q}_u)$; – · – initial design with output relocation; · · · initial design with stable inversion)

bined with a PID controller for the actuated coordinates. The stable inversion is computed from the explicitly derived internal dynamics (33), which is based on the linearly combined output (44). The stable inversion requires the numerical solution of a two-sided boundary value problem and yields a pre- and post-actuation phase. Its computation is described for a similar manipulator in [20].

The simulation results of the end-effector trajectory and the trajectory error in radial direction of the half-circular trajectory are given in Fig. 9. The simulations show that the best result is achieved by the design with optimized mass distribution of the unactuated links and using the exact end-effector position $\boldsymbol{r}^{\mathrm{ef}}(\boldsymbol{q}_a, \boldsymbol{q}_u)$

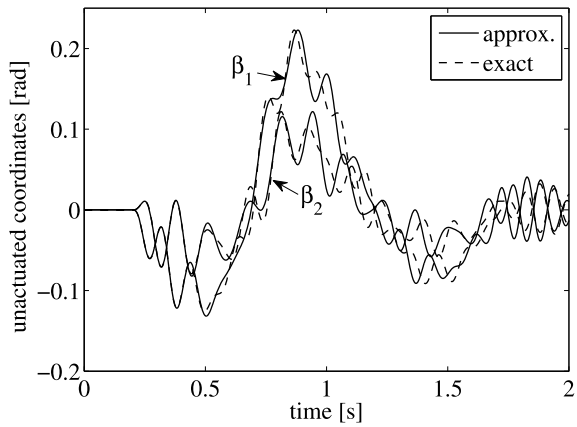

Fig. 10 Unactuated coordinates using exact and approximated output

as system output for feedback linearization. Hereby the tracking error is less than 0.002 mm. Using the linear combined output $\boldsymbol{y}$ to approximated the end-effector point $\boldsymbol{r}^{\mathrm{ef}}(\boldsymbol{y})$ yields tracking errors of approximately 2.5 mm. This is true in the case of feedback linearization of the optimized design as well as in the case of stable inversion of the non-minimum phase initial design. Finally, the simulation clearly shows that for this example output relocation is not a viable approach for end-effector trajectory tracking. Here, this results in a very large error of nearly 20 mm and is therefore not further considered. However, this approach might be useful in the case of stabilization or working point changes.

Figure 10 shows for the considered output trajectory the behavior of the unactuated coordinates β_1 and β_2 which describe the internal dynamics. It is seen that the internal dynamics for the exact end-effector position $\boldsymbol{r}^{\mathrm{ef}}(\boldsymbol{q}_a, \boldsymbol{q}_u)$ and the approximated end-effector position $\boldsymbol{r}^{\mathrm{ef}}(\boldsymbol{y})$ behaves very similar. On the one hand this justifies the use of the linear combined system output (22) for analysis and optimization of the zero-dynamics of the considered system. On the other hand, it shows that for feedback linearization the approximation can be replaced by the exact end-effector position as system output, yielding exact tracking of the end-effector trajectories.

It should be noted that the optimized design yields an increase of the total mass of the manipulator of approximately 13%. Thus, compared to the stable inversion approach the required mechanical energy for tracking the described half-circular trajectory in-

creases also by about 15%. However, the feedback linearization approach has several significant advantages compared to the stable inversion. Feedback linearization yields an algebraic control law which is relatively easy to implement and independent of the desired output trajectory. In contrast, stable inversion of a non-minimum phase system has to be computed off-line for each desired trajectory separately by the computational expensive solution of a two-sided boundary value problem, see e.g. [6, 20, 24]. Also, for the considered manipulator with passive joints the use of the exact output is much easier to implement in feedback linearization than in the stable inversion approach.

4.2 Manipulator with two passive joints: parameterization with constant mass

The previous example shows that a minimum phase design with good damping properties of the internal dynamics can be achieved by changing the mass distribution. Thereby, additional mass is added to the initial design, increasing the total mass of the system. In the two following examples, two alternative parameterizations of the mass distribution are presented which do not yield a total mass increase of the system. These parameterizations are applied to the same manipulator as in the previous example.

In the second example, a similar parameterization as in the first example, given by (45), is used. However, the total mass of the manipulator is kept constant, by reducing the mass of the passive links 3 and 4 to compensate for the additional masses m_{a_3} and m_{a_4}. Therefore, the cross section of these two links are reduced equally by the scaling factor

$$s = \frac{\bar{m}_3 + \bar{m}_4 - m_{a_3} - m_{a_4}}{\bar{m}_3 + \bar{m}_4}, \tag{46}$$

where $\bar{m}_3, \bar{m}_4$ are the masses of the initial design. Thus, the masses of the optimized links are given by $m_3 = s \cdot \bar{m}_3 + m_{a_3}$ and $m_4 = s \cdot \bar{m}_4 + m_{a_4}$, respectively. Table 3 shows for this parameterization the bounds on the parameters and the obtained optimization result. Again, it is seen that the additional masses are used to move the center of mass of the unactuated links closer to the passive joints. Figure 11 shows schematically the obtained design. The links 3 and 4 have now a squared cross section with width 37.1 mm. The good attenuation of the unactuated coordinates which is achieved by this design is shown in Fig. 12. Compared to the first example, presented in Fig. 7, this design achieves an even better damping behavior.

Table 3 Example 2—bounds and optimization results

Link 3	m_{a_3} [kg]	s_{a_3} [m]	d_{a_3} [m]
Lower bound	0	−0.333	0
Upper bound	1	0	0.167
Optimization result	1.000	−0.194	0.003
Link 4	m_{a_4} [kg]	s_{a_4} [m]	d_{a_4} [m]
Lower bound	0	−0.333	0
Upper bound	2	0	0.167
Optimization result	1.065	−0.333	0.166

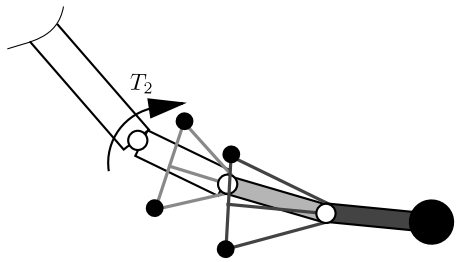

Fig. 11 Example 2: proposed design with constant mass

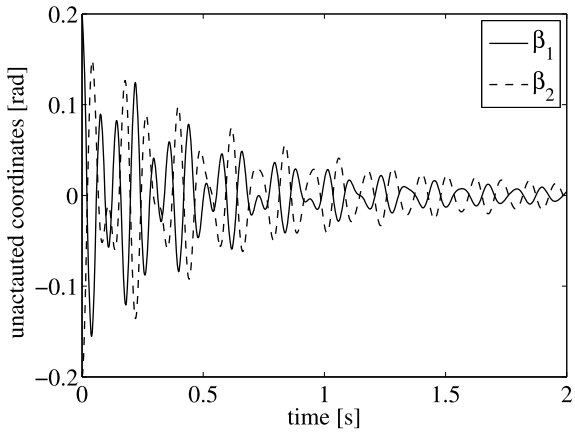

Fig. 12 Attenuation of the zero dynamics of example 2 under initial disturbance

In the third example, a parameterization with focus on changing the length of the unactuated homogeneous links l_3 and l_4 is proposed. Thereby, the length of the second link l_2 is chosen such that the total length of all three links is 1 m, i.e. $l_2 = 1m - l_3 - l_4$. How-

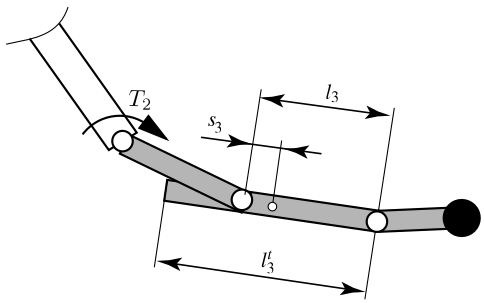

Fig. 13 Example 3: proposed design with change of link length

Table 4 Example 3—bounds and optimization results

	l_3 [m]	n_3 [–]	l_4 [m]
Lower bound	0.3	0.1	0.1
Upper bound	0.5	0.5	0.5
Optimization result	0.334	0.1	0.1

ever, it turns out that by only changing the link length no viable minimum phase design is found. Therefore, in addition to the change of the link length also the center of gravity s_3 of the third link is introduced as a design variable. This is motivated by the previous results, where the center of mass of the unactuated links is moved closer to the passive joints. Therefore, as design variables $\boldsymbol{p} = [l_3, n_3, l_4]^T$ are chosen. Thereby the factor $n_3 = s_3/l_3$ describes the relative position of the center of mass of link 3. From an engineering point of view this parameterization can be easily achieved by extending link 3 in the opposite direction, see Fig. 13. Thus the total length of the third link is given as $l_3^t = 2l_3(1 - n_3)$.

In the proposed design the links 2, 3 and 4 should have the same constant cross section. This cross section is determined from the requirement that the total mass of the three links should remain constant compared to the initial design. In order to obtain a viable physical design, bounds have to be put on the design variables. These bounds and the optimization results are summarized in Table 4. In the optimized design the third link has total length $l_3^t = 0.6$ m and the three links have squared cross section with width 44.4 mm. Figure 14 shows for this design the attenuation of the zero-dynamics under a disturbance. It is noted that this design yields a significant faster dynamic and stronger damping behavior than the previous designs. This is

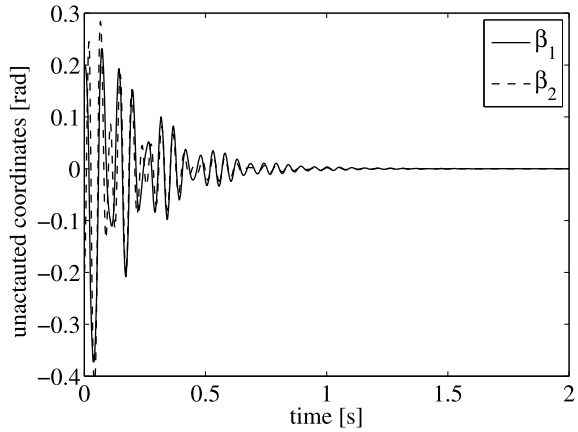

Fig. 14 Attenuation of the zero dynamics of example 3 under initial disturbance

despite the fact that the constants c, d of the spring-damper combination have not been changed.

In comparison to the previous two parameterizations of the mass distribution this third parameterization has the advantage that only 3 design variables are used. However, from the analysis of the intermediate optimization results it is seen that only few combinations of parameters yield stable designs. Thereby, the designs must be close to the bounds $n_3 = 0.1$ and $l_4 = 0.1$ m. Thus, for example always a very short link 4 is obtained.

For trajectory tracking the optimized designs in example 2 and 3 yield similar results as in the first example shown in the previous section. However, the required mechanical energy is now within 2% of the stable inversion result of the initial design. This is due to the constant mass parameterization of the mass distribution in these two examples. This clearly demonstrates that minimum phase designs with good damping properties can be achieved without a total mass increase.

4.3 Manipulator with four passive joints

As last example, the design of an underactuated manipulator with four passive joints is considered, see Fig. 15. The actuated generalized coordinates are again $\boldsymbol{q}_a = [x, \alpha_1, \alpha_2]^T$ and the unactuated generalized coordinates are now $\boldsymbol{q}_u = [\beta_1, \beta_2, \gamma_1, \gamma_2]^T$. These are again defined as relative joint coordinates. Thereby β_1 is the angle between link 1 and 2, β_2 is the angle between link 2 and 3, γ_1 is the angle between link 4 and 5

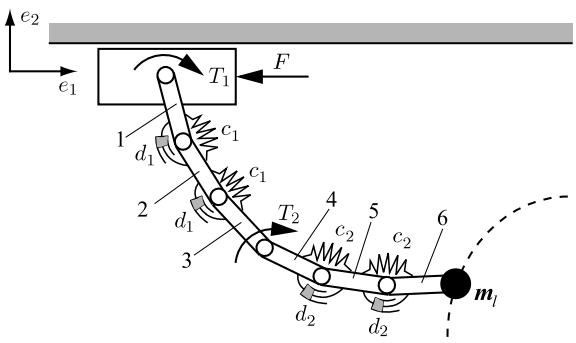

Fig. 15 Underactuated manipulator with four passive joints

Table 5 Initial parameters for underactuated manipulator with four passive joints

Cart	$m_c = 3$ kg		
Link $i = 1$–6	$m_i = 2.292$ kg	$I_i = 0.0217$ kgm^2	$l_i = 1/3$ m
Load	$m_l = 6$ kg	$I_l = 0.0147$ kgm^2	
$c_1 = 900\ \frac{\text{Nm}}{\text{rad}}$	$c_2 = 300\ \frac{\text{Nm}}{\text{rad}}$	$d_1 = 3\ \frac{\text{Nms}}{\text{rad}}$	$d_2 = 1\ \frac{\text{Nms}}{\text{rad}}$

and γ_2 is the angle between link 5 and 6. The manipulator is actuated by the control input $\boldsymbol{u} = [F, T_1, T_2]^T$. The physical properties are summarized in Table 5. The links are homogeneous and have again a squared cross section with initial width 50 mm. For the analysis and optimization of the internal dynamics the end-effector point $\boldsymbol{r}^{\text{ef}}$ is described approximately by using the linearly combined system output

$$\boldsymbol{y} = \boldsymbol{q}_a + \boldsymbol{\Gamma}\boldsymbol{q}_u \quad \text{with } \boldsymbol{\Gamma} = \begin{bmatrix} 0 & 0 & 0 & 0 \\ 2/3 & 1/3 & 0 & 0 \\ 1/3 & 2/3 & 2/3 & 1/3 \end{bmatrix}. \tag{47}$$

As in the previous examples, the manipulator moves in the horizontal plane and there are infinity equilibrium points. In this example the zero-dynamics depends indeed on the values y_2, y_3, however, inspection shows that their influence is rather small. Thus, the analysis and optimization can be performed at one equilibrium point and holds for the entire range. Therefore, in the following it is chosen $y_2 = y_3 = 0$. The analysis of the zero-dynamics shows that its stability depends on the mass distribution of the links 2–6. However, it turns out that for this example it is sufficient to change the mass distribution of the links 2, 3, 5 and 6. In this example the same approach

Table 6 Example 4—bounds and optimization results

Link 2	m_{a_2} [kg]	s_{a_2} [m]	d_{a_2} [m]
Lower bound	0	−0.667	0
Upper bound	3	0	0.333
Optimization result	1.6127	−0.2067	0.3019
Link 3	m_{a_3} [kg]	s_{a_3} [m]	d_{a_3} [m]
Lower bound	0	−0.667	0
Upper bound	3	0	0.333
Optimization result	2.4230	−0.6349	0.2778
Link 5	m_{a_5} [kg]	s_{a_5} [m]	d_{a_5} [m]
Lower bound	0	−0.667	0
Upper bound	2	0	0.333
Optimization result	0.8381	−0.1824	0.0865
Link 6	m_{a_6} [kg]	s_{a_6} [m]	d_{a_6} [m]
Lower bound	0	−0.667	0
Upper bound	2	0	0.167
Optimization result	1.5187	−0.3011	0.0096

as in example 2 is used. Thus, additional masses m_{a_i} at position s_{a_i} and d_{a_i} are introduced for these four links. The total mass of the manipulator is kept constant and it is required that all 6 links have equal cross section. Table 6 shows the bounds on the parameters and the obtained optimization result. In this case 300 particles and 10 iterations are used in the particle swarm optimization, requiring approximately 45 min computation time. The links have now a squared cross section with width 36.6 mm. Figure 16 shows that with this design a good and equal attenuation of an initial disturbance in the zero dynamics is obtained.

The obtained manipulator is tested using the trajectory presented in Fig. 8. Thereby feedback linearization with the exact end-effector position $\boldsymbol{r}(\boldsymbol{q}_a, \boldsymbol{q}_u)$ as system output is used. By simulation it is shown that the obtained internal dynamics is also robust to parameter uncertainty and measurement noise. Therefore, in the simulation model the mass of the load is increased by 10%, the stiffness of the springs are increased by 15% and the damping coefficients are reduced by 30%. Also measurement noise is added to all generalized coordinates. While in the nominal case a negligible tracking error occurs, a small tracking error of 0.338 mm occurs for the simulation with disturbances and uncertainties. Figure 17 shows for the

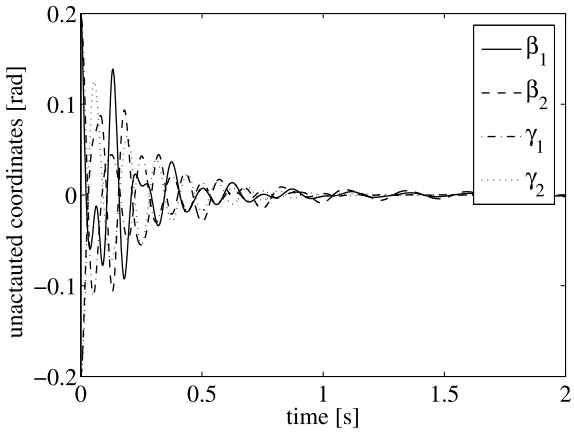

Fig. 16 Attenuation of the zero dynamics of example 4 under initial disturbance

desired output trajectory the behavior of the unactuated generalized coordinates which describe the internal dynamics. It is seen that the internal dynamics remains bounded for the nominal model as well as for the model with uncertainties and disturbances. This indicates that the minimum phase property of the designed system is robust against some uncertainties and disturbances. While a rigorous robustness proof is beyond the scope of this paper, the obtained designs show in simulation promising robustness properties and might be the starting point for further reaching investigations. These designs might also be the basis for further control concepts with good robustness properties, such as passivity-based control or sliding-mode control, which generally require minimum phase systems.

5 Conclusions

An integrated approach for design and control of minimum phase underactuated multibody systems is presented. Thereby, systems with stable zero dynamics and good damping properties of the zero dynamics are designed by optimization. As design parameters, which influence the zero dynamics, the geometric dimensions and mass distribution of the system are identified. The mass distribution can be influenced by small masses, which are added to the unactuated bodies, whereby the parameterization can be chosen in such a way that no increase of the total mass occurs. For the optimization a particle swarm algorithm

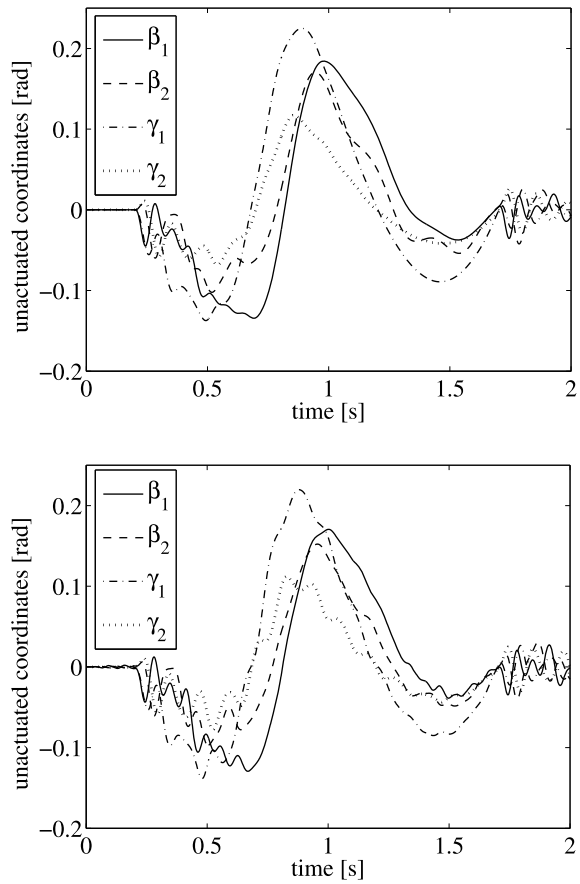

Fig. 17 Unactuated coordinates during trajectory tracking without (*top*) and with (*bottom*) uncertainties and disturbances

is used. The two-step optimization criteria calculation yields a time efficient optimization procedure which provides reliable results. For the analysis and optimization of the zero dynamics the end-effector point is approximated by a linearly combined output. However, the presented optimization procedure is general and not restricted to such system outputs. The efficiency of the approach is demonstrated by simulation using planar underactuated manipulators with two and four passive joints, respectively. For the obtained minimum phase systems feedback linearization is possible, and also feed-forward control design is significantly simplified.

Acknowledgements The author would like to thank the German Research Foundation (DFG) for financial support of the project within the Cluster of Excellence in Simulation Technology (EXC 310/1) at the University of Stuttgart.

References

1. Agrawal, S., Sangwan, V.: Differentially flat designs of underactuated open-chain planar robots. IEEE Trans. Robot. **24**, 1445–1451 (2008)
2. Ast, A., Eberhard, P.: Flatness-based control of parallel kinematics using multibody systems—simulation and experimental results. Arch. Appl. Mech. **76**, 181–197 (2006)
3. Blajer, W., Kolodziejczyk, K.: A geometric approach to solving problems of control constraints: theory and a DAE framework. Multibody Syst. Dyn. **11**, 343–364 (2004)
4. Brockett, R.: Feedback invarianta for nonlinear systems. In: Proceedings of the 7th IFAC World Congress, Helsinki (1978)
5. De Luca, A.: Trajectory control of flexible manipulators. In: Siciliano, B., Valavanis, K. (eds.) Control Problems in Robotics and Automation, pp. 83–104. Springer, London (1998)
6. Devasia, S., Chen, D., Paden, B.: Nonlinear inversion-based output tracking. IEEE Trans. Autom. Control **41**, 930–942 (1996)
7. Isidori, A.: Nonlinear Control Systems. Springer, London (1995)
8. Kennedy, J., Eberhart, R.: Particle swarm optimization. In: Proceedings of the International Conference on Neural Networks, Perth, pp. 1942–1948 (1995)
9. Kennedy, J., Eberhart, R.: Swarm Intelligence. Morgan Kaufmann, San Francisco (2001)
10. Khalil, H.: Nonlinear Systems. Prentice Hall, Upper Saddle River (2002)
11. Li, Z., Yang, Y., Wang, S.: Adaptive dynamic coupling control of hybrid joints of human-symbiotic wheeled mobile manipulators with unmodelled dynamics. Int. J. Soc. Robot. **2**, 109–120 (2010)
12. Moallem, M., Patel, R., Khorasani, K.: Flexible-link Robot Manipulators: Control Techniques and Structural Design. Springer, London (2000)
13. Sastry, S.: Nonlinear Systems: Analysis, Stability and Control. Springer, New York (1999)
14. Sedlaczek, K.: Zur Topologieoptimierung von Mechanismen und Mehrkörpersystemen. Schriften aus dem Institut für Technische und Numerische Mechanik der Universität Stuttgart. Shaker Verlag, Aachen (2007) (In German)
15. Sedlaczek, K., Eberhard, P.: Using augmented Lagrangian particle swarm optimization for constrained problems in engineering. Struct. Multidiscip. Optim. **32**, 277–286 (2006)
16. Seifried, R.: Optimization-based design of feedback linearizable underactuated multibody systems. In: Proceedings of the ECCOMAS Thematic Conference Multibody Dynamics 2009, Warsaw (2009). Paper ID 121
17. Seifried, R.: Optimization-based design of minimum phase underactuated multibody systems. In: Blajer, W., Arczewski, K., Fraczek, J., Wojtyra, M. (eds.) Multibody Dynamics: Computational Methods and Applications. Computational Methods in Applied Sciences, vol. 23, pp. 261–282. Springer, Berlin (2011)
18. Seifried, R., Held, A., Dietmann, F.: Analysis of feedforward control design approaches for flexible multibody systems. J. Syst. Des. Dyn. **5**, 429–440 (2011)
19. Seifried, R.: Two approaches for feedforward control and optimal design of underactuated multibody systems. Multibody Syst. Dyn. doi:10.1007/s11044-011-9261-z
20. Seifried, R., Eberhard, P.: Design of feed-forward control for underactuated multibody systems with kinematic redundancy. In: Ulbrich, H., Ginzinger, L. (eds.) Motion and Vibration Control: Selected Papers from MOVIC 2008, pp. 275–284. Springer, Munich (2009)
21. Skogestad, S., Postlethwaite, R.: Multivariable Feedback Control. Wiley, Chichester (2005)
22. Soltine, J.-J., Li, W.: Applied Nonlinear Control. Prentice Hall, Englewood Cliffs (1991)
23. Spong, M., Hutchinson, S., Vidyasagar, M.: Robot Modeling and Control. Wiley, Hoboken (2006)
24. Taylor, D., Li, S.: Stable inversion of continuous-time nonlinear systems by finite-difference methods. IEEE Trans. Autom. Control **47**, 537–542 (2002)